SEMARAK ILMU PUBLISHING

CFD Letters

Journal homepage:
https://semarakilmu.com.my/journals/index.php/CFD_Letters/index
ISSN: 2180-1363


# Numerical Investigation on the Conical Flow of Viscoelastic Fluids

Ahmed M. Shareef[1,*], Alaa H. Al-Muslimawi[1]

[1] Department of Mathematics, College of Science, University of Basrah, Basrah, Iraq

**ARTICLE INFO**

***Article history:***
Received 15 June 2023
Received in revised form 18 July 2023
Accepted 21 August 2023
Available online 1 January 2024

***Keywords:***
Galerkin method; Hybrid finite element/volume scheme; Phan–Thien/Tanner model; Stick-slip; Viscoelasticity

**ABSTRACT**

The conical problem represents one of the important problems in the various fields of industrial as the automotive industry and the aerospace industry, due to their great role in controlling the flow of liquids and gases. This article covers a computational investigation of incompressible the Phan–Thien/Tanner shear-thinning viscoelastic fluid flow through a conical converging channel. Here, we select hybrid finite element/finite volume algorithm as a first time to treat such problem. This method consists of the combination of a Taylor-Galerkin/pressure correction finite element method (TGPC-FEM) and a cell-vertex finite volume approach (CV-FEA) to solve the system of partial differential equations that govern the fluid flow. The TGPC-FEM is employed to the momentum and mass conservation models, while the stress constitutive models are treated by finite volume implementation. The findings of current study are concerned with stress response, deformation rate, and pressure drop under variations in Weissenberg number and EPTT parameters. The effect of shear-thinning behaviour with the EPTT representation is also considered.

## 1. Introduction

One of the most fascinating phenomena is the shear-thinning viscoelastic flow through the conical, which is extensively studied in the computational fluid dynamics. Practically, conical fluid flow refers to the flow of a fluid through a conical-shaped conduit or channel, and it is a common phenomenon encountered in various engineering applications and fluid dynamics studies. In fact, the behavior of fluid flow in a conical channel is influenced by factors such as the inlet conditions, geometry of the conduit, fluid properties, and any external forces acting on the flow. In addition, conical fluid flow finds applications in various fields such as the design of nozzles, diffusers, ejectors, converging-diverging ducts, and fluidic systems. In this domain analytical methods, numerical simulations, and experimental techniques are employed to study and analyses conical fluid flow behavior in practical applications.

Relationships regarding incompressible conical flow can be formulated back to the early 20th century, where the analytical solutions for creeping Newtonian flow are presented by Harrison [1] and Bond [2]. In these studies, the velocity and pressure fields and Harrison studied the velocity field, and Bond found the pressure field are extensively studied. However, the obtained solutions assume

* *Corresponding author.*
*E-mail address: ahmad.muhamad.sci@uobasrah.edu.iq (Ahmed M. Shareef)*

https://doi.org/10.37934/cfdl.16.4.8597

a purely radial flow throughout which the flow at the inlet and outlet of the cone cannot be modified. Or the conical flow analysis of energy law fluids Oka and Takami [3] used the creeping radial flow, where the provided an ordinary differential equation for the velocity field; however, unlike Harrison, they did not establish an analytic or numerical solution to the equation. Forsyth [4] later concluded that the assumption of radial flow constrains Harrison and Bond solutions to small-angle cones. Some studies have discussed non-Newtonian fluids. Moreover, Sutterby [5] studied the effect of the angles and diameter ratio on the flow. There, the author found out that the small diameter ratio and small angles generate only slight normal elastic pressures in the flow. By ignoring the inertia, *Kwon et al.,* [6], and Kajiwara *et al.,* [7] employed the finite element method for the first time to analyze the conical flows. In contrast, the finite difference method is has been used by Jarzebski and Wilkinson [8] to study inelastic fluid in a conical channel using a power law model, including inertia. They obtained data on evolution length, stress evolution and pressure drop. However, their findings are limited to light-shear fluids and small conical angles. Furthermore, they did not use fluxes to enter or exit the conical duct. These studies had been achieved when inertia was neglected. In addition, many accomplished research papers include converging flow had been published (see for example [9–12]). In fact, the study of viscoelastic flows represents a high challenge in the field of fluid dynamics. Particularly, for a circular conical viscoelastic problem, few studies have been conducted. Thus, in this article we concerned with the study of viscoelastic solutions for axisymmetric conical problem under isothermal condition, by appealing to the exponential Phan-Thien Tanner (EPTT) viscoelastic models, with properties of shear-thinning and moderate-high Trouton ratios.

Given the importance of studying conical problem due to of its wide applications, we have highlighted its numerical solutions. Basically, the conical flows play an essential role in effective fields including irrigation, hydraulic systems, and transportation. In addition, providing a numerical method with high accuracy will be of great importance in providing an important aid in finding many of the problems that confront researchers in these areas. For these reasons, this study concerned in this type of scientific issue.

The novelty of this work is to treat the conical viscoelastic problem by using hybrid of finite element and finite volume methods, which did not use previously for such problem. Here, a Taylor-Galerkin/ pressure correction method (TG-PC-M) is employed to solve the continuity and momentum equations, while the stress constitutive model is treated by invoking a cell-vertex fluctuation distribution finite volume method for more details about such method (see Ref. [13,14]). Here, particular attention is paid to study the effect of some parameters, such as the viscoelasticity (*We*) and the used constitutive model on the solution components. In addition, the difference of the geometric parameters influences the distribution of the static pressure and the drag force, which in turn influences the mass flow rate at the outlet.

In the next section, the mathematical model and constitutive model of the viscoelastic fluid flow will be introduced. The discretization method that utilized to treat the governing equations will be introduced in Eq. (3). The problem specification, material functions and the numerical results will be presented in Eq. (4), (5) and (6), respectively.

## 2. Mathematical Equations and Constitutive Models

The fundamental governing equations of the incompressible viscoelastic fluid flow are presented in this section. These equations consist of continuity, momentum and stress constitutive equation, which are expressed in the following forms [15-18]:

$$\nabla \cdot \boldsymbol{u} = 0. \tag{1}$$

$$\rho \frac{\partial u}{\partial t} = \nabla(-pI + 2\mu_s d + \tau) - \rho u \cdot \nabla u \tag{2}$$

Where, u, ρ, τ and p represent fluid velocity, fluid density, the polymeric contribution to the extra-stress tensor and hydrodynamic pressure, respectively. In addition, (d=(∇u + (∇u)T )/2)is the rate-of-deformation and (μs) represents a solvent component of viscosity. Furthermore, the EPTT model can be obtained as follows:

$$We\ \partial\tau/\partial t = (2(1-\beta)d - f(\tau)\tau) - We(u \cdot \nabla\tau) + We(1-\xi)(\nabla u^{\dagger} \cdot \tau + \tau \cdot \nabla u) \tag{3}$$

Here, *We* is the Weissenberg number and $f$ represents the nonlinear function expressed as

$$f(\tau) = \exp\left(\frac{\varepsilon_{EPTT}\, We}{(1-\beta)} tr(\tau)\right). \tag{4}$$

The constant $\varepsilon_{PTT}$ and $\xi$ are material parameters of the non-dimensional model.

## 3 Numerical Method

### *3.1 Taylor–Galerkin Pressure Correction Discretization*

The $TG{-}PC{-}FEM$ algorithm is presented to treat the system of current governing equations. This algorithm was suggested by Townsend and Webster [19]. A Taylor–Galerkin scheme based on two-step Lax–Wendroff and a pressure-correction scheme represent the general framework of this algorithm. In contrast, a second-order accuracy in time by adopting a semi-implicit Crank–Nicolson time split with the time increment factor $\theta_{cr}$ is the main base of the pressure-correction method. The stages of this algorithm are gathered as follows:

Stage 1a: - $\frac{2Re}{\Delta t}\left[u^{n+\frac{1}{2}} - u^n\right] = [\nabla.(\tau + 2\beta d) - Reu.\nabla u - \nabla p]^n$ , (5)

$$\frac{2We}{\Delta t}\left[\tau^{n+\frac{1}{2}} - \tau^n\right] = [2(1-\beta)d - \tau + We(\nabla u.\tau + \tau.(\nabla u)^T]^n \text{ ,} \tag{6}$$

Stage 1b: - $\frac{Re}{\Delta t}[u^* - u^n] = [\nabla.(\tau + 2\beta d) - Re\ u.\nabla u]^{n+\frac{1}{2}}$ - $\nabla p^n$, (7)

$$\frac{We}{\Delta t}[\tau^{n+1} - \tau^n] = [\,2(1-\beta)d - \tau + We(\nabla u.\tau + \tau.(\nabla u)^T]^{n+\frac{1}{2}}\text{ ,} \tag{8}$$

Stage 2: - $\nabla^2(p^{n+1} - p^n) = \frac{Re}{\theta_{cr}\Delta t}\ \nabla.u^*$, (9)

Stage 3: -$u^{n+1} = u^* - \frac{\theta_{cr}\Delta t}{Re}[\nabla(p^{n+1} - p^n)]$, (10)

In these fractional stages, velocity and stress fields are calculated at the half time step $(u,\tau)^{n+\frac{1}{2}}$ and corrected for the full time step $(u^*,\tau)^{n+\frac{1}{2}}$ ($Stage$ 1). The momentum diffusion term is treated in a semi-implicit way to improve the convergence and stability of the solution. The velocity field ($u^*$), which is derived through the full time step of the momentum, may not satisfy continuity

and require correction. Thus, a Poisson-like equation is generated to increase the time step of pressure ($Stage$ 2) accompanied with a correction ($Stage$ 3).

### *3.2 Sub-vertex Finite Volume Discretization*

The stress constitutive is rewritten into a conservative form and the flux ($R$) and source ($Q$) terms are identified to outline the application of $fv$ theory:

$$\partial\tau/\partial t = -(u\tau) + (\frac{1}{We}(2(1-\beta)d-\tau) + \nabla u.\tau + \tau.\nabla u) \quad (11)$$

The cell-vertex $fv$ approaches are achieved for Eq. (11) through fluctuation distribution as an upwinding strategy to distribute control volume residuals and furnish nodal solution updates [20-23]. Each scalar stress component, $\tau$, is considered to be acting on an arbitrary volume Ω = $\sum l$ Ω, whose variation is controlled by the corresponding fluctuation components of the flux ($u\tau$) and the source ($\frac{1}{We}(2(1-\beta)d-\tau) + \nabla u^T.\tau + \tau.\nabla u$):

$$\partial/\partial t \int \Omega l\ \tau d\Omega = -\int \Omega l\ R d\Omega + \int \Omega l\ Q d\Omega \quad (12)$$

The integral source variations and flux are calculated over each finite volume triangle (Ω) and appropriated proportionally by the chosen cell-vertex distribution method to its three vertices. The update of nodal is gained by summing all contributions from its control volume Ω composed of all $fv$ triangle surrounding nodes ($l$). Moreover, the flux and source residuals are probably determined through two separate control volumes associated with a given node ($l$) within the $fv$ cell $T$, generating two contributions: one is upwinded and governed over the $fv$ triangle $T$, ($(u\tau)T$, $\frac{1}{(We}(2(1-\beta)d-\tau) + \nabla u^T.\tau + \tau.\nabla u\ )T$), and the other is area averaged and subtended over the median dual-cell zone ($RMDC$, $QMDC$). For the reasons of temporal accuracy, this procedure demands appropriate area weighting to maintain consistency with extension to time terms likewise. In this context, a generalized $fv$ nodal update equation is derived per stress component by separating the treatment of individual time derivative, flux, and source terms and integrating the associated control volumes given as;

$$\sum_{\forall T_l} \delta_T \alpha_l^T \Omega_T + \sum_{\forall MDC_l} (1-\delta_T)\Omega_l^T] \frac{\Delta\tau_l^{n+1}}{\Delta t} = \sum_{\forall T_l} \delta_T \alpha_l^T b^T + \sum_{\forall MDC_l} (1-\delta_T) b_l^{MDC}, \quad (13)$$

Where $b^T$= ($-RT + QT$), $b_l^{MDC}$= $(-\mathrm{RMDC} + \mathrm{QMDC})^l$, $\Omega^T$is the area of the $fv$ triangle $T$, and (10 × 20) element is the area of its median dual-cell ($MDC$). The weighting parameter, 0 ≤ $\delta_T$≤ 1, balances the proportions taken between the contributions from the median dual cell and $fv$ triangle $T$. The discrete stencil (18) identifies fluctuation distribution, median dual-cell contributions, area weighting, and upwinding factors ($\alpha_l^T$scheme dependent) [24-27].

### *3.3 Low Diffusion $\mathcal{B}$ Scheme*

Aboubacar *et al.,* [21] and Al-Muslimawi *et al.,* [23] showed the approach of low diffusion $B$ ($LDB$) is appropriate option to find the fluctuation distribution parameter $\alpha$. It is a linear method with the properties of second-order linear preservation and accuracy. The $LDB$ distribution coefficients $\alpha i$ are

determined in each triangle via angles $\gamma 1$ and $\gamma 2$, subtended at an inflow vertex ($i$) by the advection velocity $a$, where $a$ is the average of velocity field per $fv$ cell:

$$\boldsymbol{\alpha_i = \frac{sin\gamma_1 cos\gamma_2}{sin(\gamma_1+\gamma_2)}}\ , \boldsymbol{\alpha_j = \frac{sin\gamma_2 cos\gamma_1}{sin(\gamma_1+\gamma_2)}}\ , \boldsymbol{\alpha_k = 0}\ . \tag{14}$$

If $\boldsymbol{\gamma_1 > \gamma_2}$, then $\boldsymbol{\alpha_i > \alpha_j}$; thus, by design, the contribution of the flow from node ($i$) is greater than that of the flow from node ($j$).

Additionally, the setting of boundary condition (BCs) of the current problem with is given as:

i. The chosen inflow conditions are those corresponding to the analytical expression of fully developed axial velocity and zero radial velocity.
ii. No-slip boundary condition is applied to the top and bottom walls of channels.
iii. Zero radial velocity and zero pressure are applied to the outlet of channels.
iv. The radial velocity along the axisymmetric line is removed.

## 4. Problem Specification

The problem in this study is chosen to be a cone connected to upstream and downstream cylinders. In this context, a Poiseuille flow through a 2D axisymmetric conical channel [1:0.5, 2:0.5, 3:0.5 and 4:0.5] is considered for an isothermal incompressible viscoelastic fluid. The radius of the upstream tube is selected to be twice the downstream tube width. Figure 1(a) illustrates the schematic of such a benchmark flow problem. A triangular finite element mesh called C-M is used with a half angle of α = 30°, as shown in Figure 1. Table 1 and 2 presents further details about the mesh characteristics.

**Table 1**
Geometry (C-M) dimensions

| Dimension | Measures |
|---|---|
| L1 | 4 |
| L2 | 1 |
| L3 | 1 |
| L4 | 6 |
| R1 | 1 |
| R2 | 0.5 |

**Table 2**
Geometry (C-M) dimensions

| Dimension | Measures |
|---|---|
| Elements | 128 |
| Nodes | 97 |
| Boundary nodes | 80 |

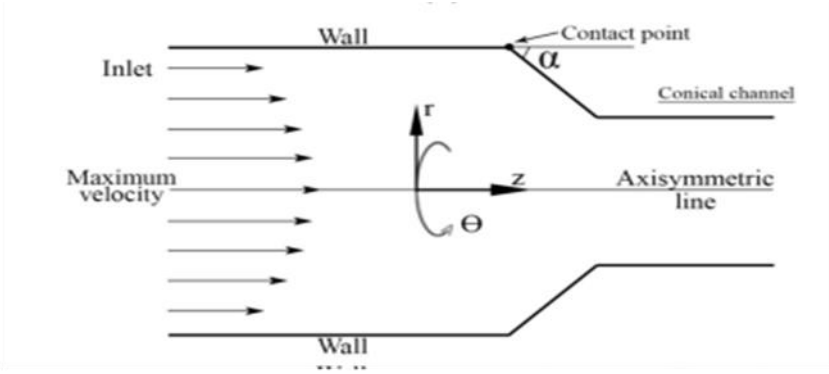


(a)

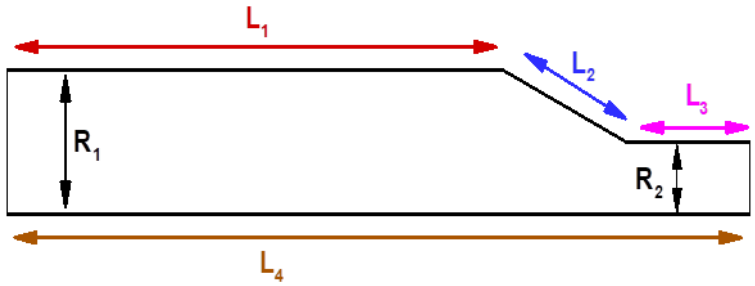


(b)

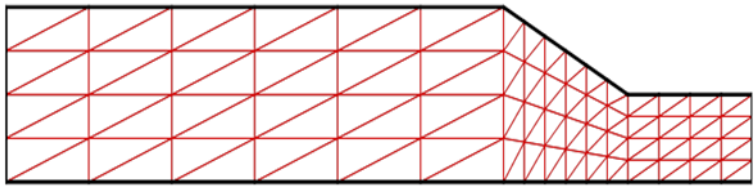

(c)

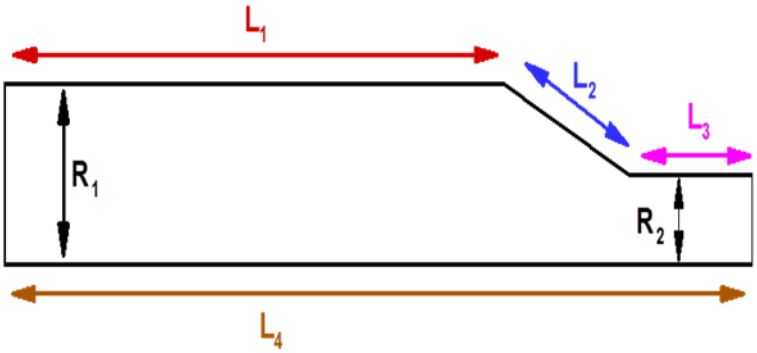


(d)

**Fig. 1.** Schematic and finite element mesh (C-M) for conical

## 5. Results and Discussion

In this study, the numerical solutions of a viscoelastic conical flow are presented through various key parameters of the EPTT model ($\varepsilon_{\mathrm{EPTT}} = 0.02, 0.15, 0.25$) and the solvent fraction ($\beta = 0.9$) with variation in Weissenberg number.

### *5.1 Effect of We Variation*

Figure 2 illustrates the pressure drop plot for a Newtonian case and viscoelasticity with *We* = {1, 5, 10} along the axis of symmetry. The profiles show that *We* affects pressure distribution in channels. In this context, the level of pressure drop increases gradually as *We* increases because of the shear-thinning behaviour. Here, the maximum level of pressure of a Newtonian flow is reached compared with viscoelasticity through the channel zone. By comparison, no change is observed in the cone section.

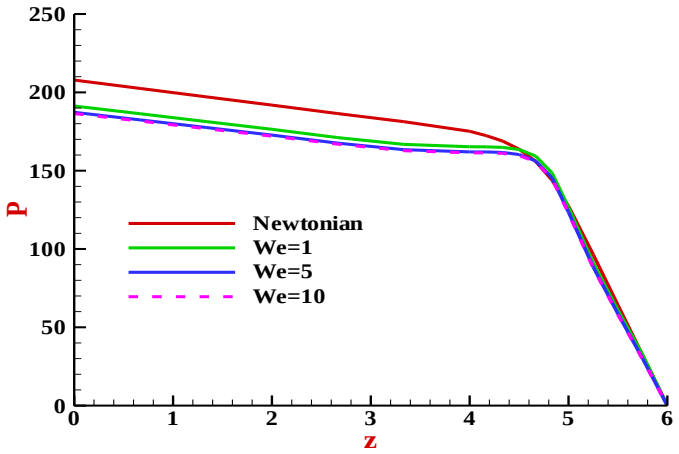


**Fig. 2.** Pressure drops along centerline: EPTT$\{\varepsilon_{\mathrm{EPTT}} = 0.02, \xi_{\mathrm{EPTT}} = 0.0\}$, $\beta = 0.9$, $We$ variation

The radial stress ( $\tau_{rr}$) in the top and centreline zones is displayed in Figures 3(a–b) for EPTT $\{\varepsilon_{\mathrm{EPTT}} = 0.02, \xi_{\mathrm{EPTT}} = 0.0\}$ and $We = \{1,5,10\}$ at fixed $\beta = 0.9$. The profiles show that the magnitude in the cone area significantly increases as *We* decreases. The findings reveal that an overshoot exists in pre- and post-cone exit regions with a maximum level at *We* = 1. Figure4 presents more details of the zoned part of the cone.

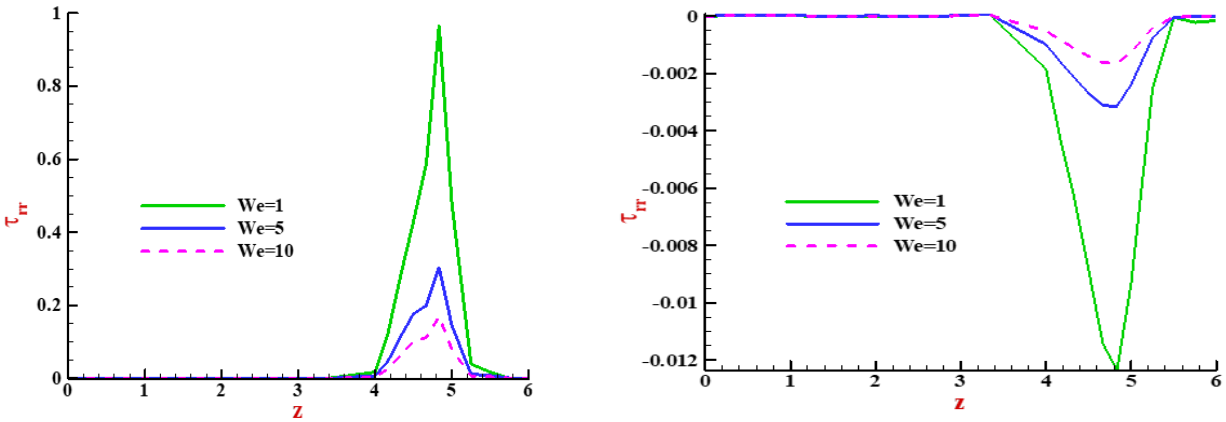


(a) Top surface (b) Centreline

**Fig. 3.** Radial stress ($\tau_{rr}$), *EPTT*$\{\varepsilon_{\mathrm{EPTT}} = 0.02, \xi_{\mathrm{EPTT}} = 0.0\}$: $\beta = 0.9$, $We$ variation

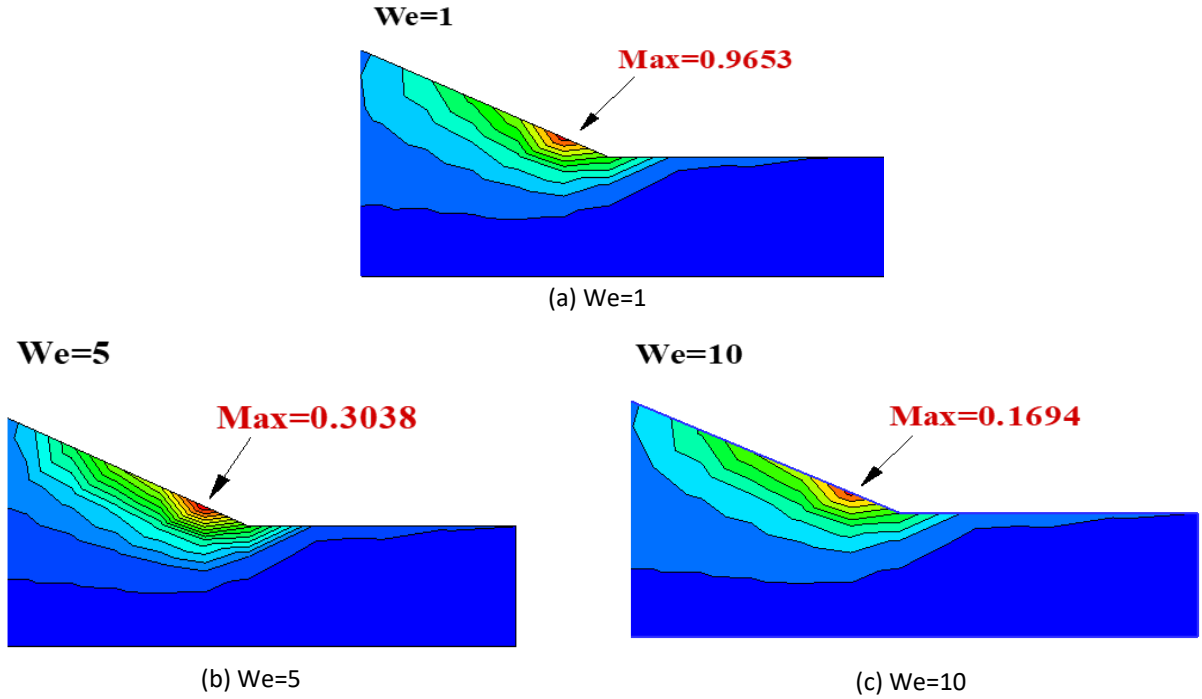


(a) We=1

(b) We=5

(c) We=10

**Fig. 4.** Axial stress ($\tau_{rr}$) fields in the cone zone, EPTT$\{\varepsilon_{\mathrm{EPTT}} = 0.02, \xi_{\mathrm{EPTT}} = 0.0\}$: $\beta = 0.9$, $We$ variation

Figure 5 illustrates normal stress ($\tau_{ZZ}$) along the axis of symmetry under the same set of parameters. Constant normal stress levels occur along the die section and cone exit. They increase and then sharply decrease in the cone section. In this case, normal stress increases as *We* decreases because of the influence of shear-thinning behaviour with the EPTT representation. For instance, on the top surface with *We* = 1, the maximum $\tau_{zz}$ is around 12 units; by comparison, the maximum $\tau_{zz}$ at *We* = 10 is 2 units, which is almost *O*(83%) reduction. In addition, $\tau_{ZZ}$ on the top surface is much higher than that in the centreline. Specifically, Figure 6 presents the field structures of axial normal stress in the cone section for three different values of *We* = {1, 5, 10}, $\beta = 0.9$, and $\varepsilon_{\mathrm{EPTT}} = 0.02$. The fields show that the maxima of $\tau_{zz}$ occurs at the zone of the drawdown section. Normal stress decreases as *We* increases.

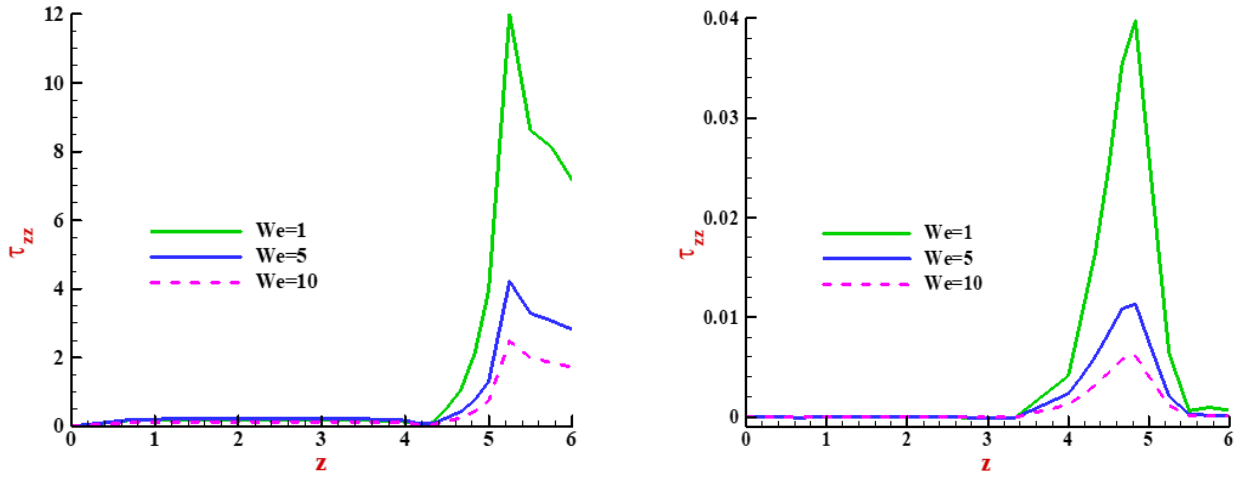


(a) Top surface

(b) Centreline

**Fig. 5.** Normal stress ($\tau_{zz}$), EPTT$\{\varepsilon_{\mathrm{EPTT}} = 0.02, \xi_{\mathrm{EPTT}} = 0.0\}$: $\beta = 0.9$, $We$ variation

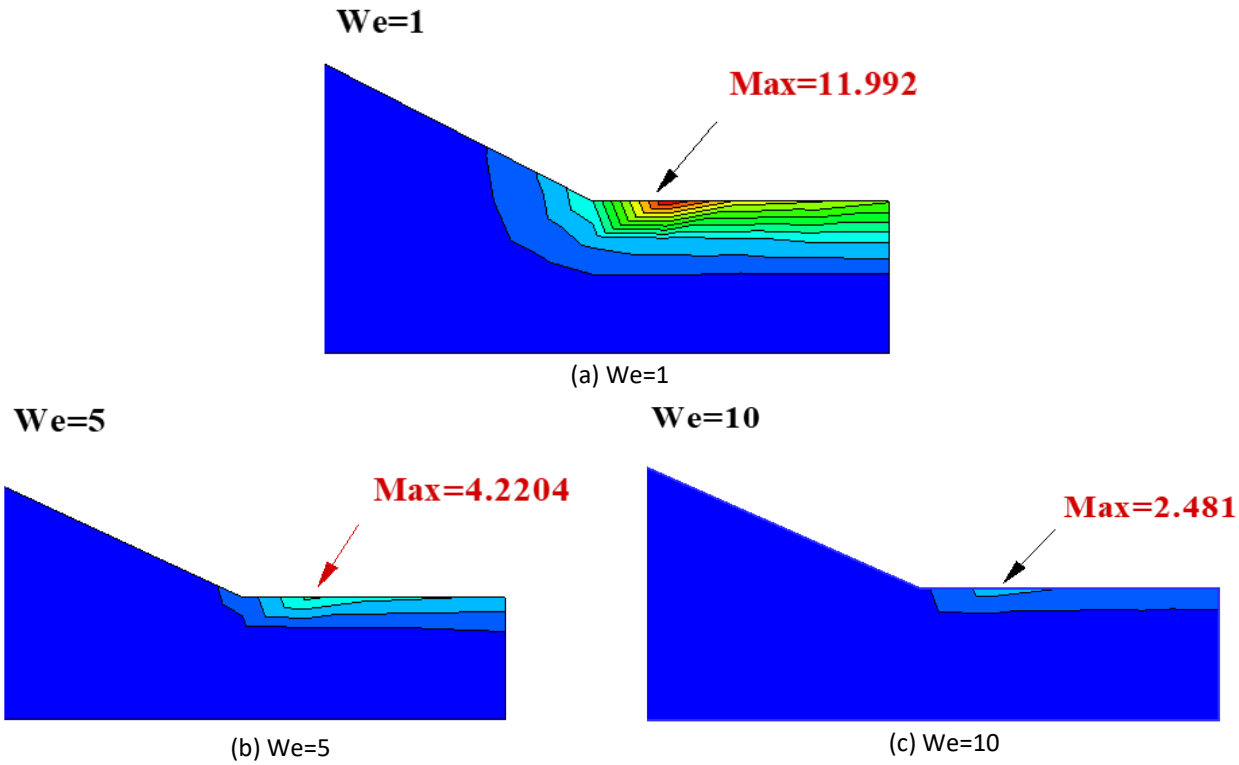


(a) We=1

(b) We=5

(c) We=10

**Fig. 6.** Normal stress ($\tau_{zz}$) field, *EPTT*$\{\varepsilon_{\mathrm{EPTT}} = 0.02, \xi_{\mathrm{EPTT}} = 0.0\}$: $\beta = 0.9$, $We$ variation

Figure 7 plots the shear data, with shear stress ($\tau_{rz}$) along the top surface of the conical for the same parameter settings. The findings reveal that relaxation that is apparent through the channel region with a shear component almost vanishes. In the cone region, an opposing feature from normal stress is indicated by a peak shear in magnitude observed at *We* = 1.

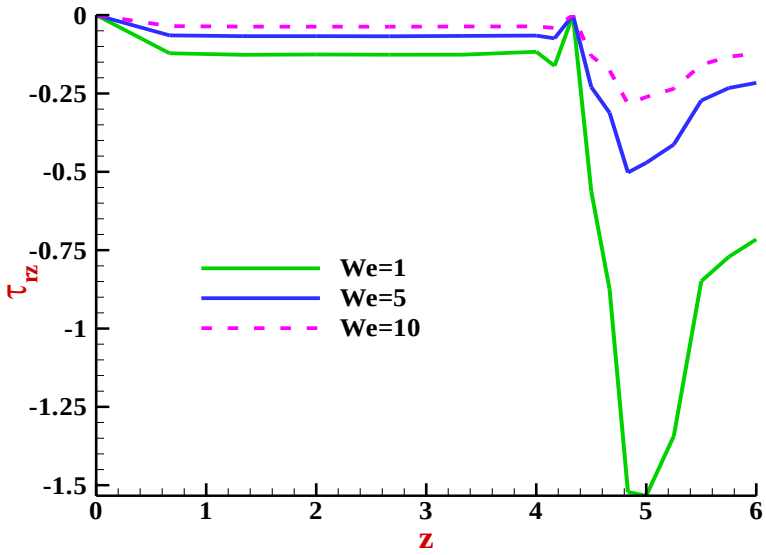


**Fig. 7.** Shear stress ($\tau_{rz}$) along the top wall,
EPTT$\{\varepsilon_{\mathrm{EPTT}} = 0.02, \xi_{\mathrm{EPTT}} = 0.0\}$: $\beta = 0.9$, $We$ variation

### *5.2. Effect of $\varepsilon_{EPTT}$ Variation*

For more details, Figure 8 illustrates the pressure profiles along the centreline at *We* = 1 and through variation in the $\varepsilon_{\mathrm{EPTT}}$ ratio. This result indicates the largest pressure in both regions at $\varepsilon_{\mathrm{EPTT}}$ = 0.02. The pressure drop slightly decreases as the $\varepsilon_{\mathrm{EPTT}}$ ratio increases from $\varepsilon_{\mathrm{EPTT}}$ = 0.02 to $\varepsilon_{\mathrm{EPTT}}$ = 0.25, which reflects the shear-thinning impact.

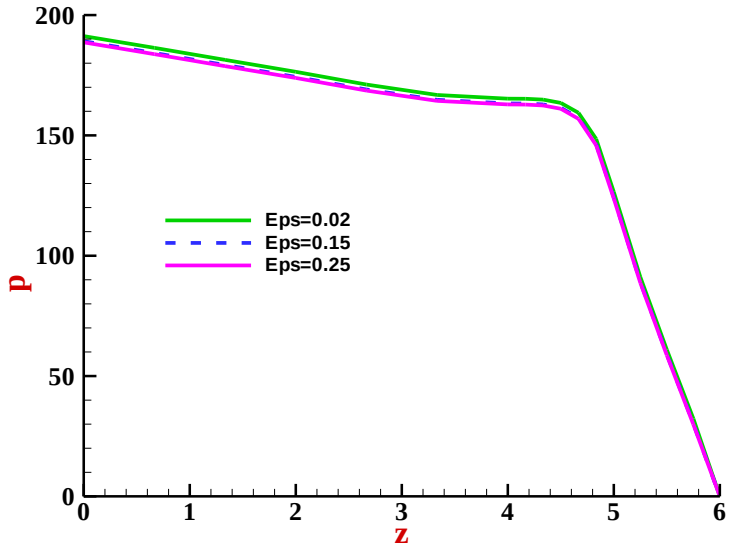


**Fig. 8.** Pressure drops along centreline: EPTT$\{We = 1, \xi_{\mathrm{EPTT}} = 0.0\}$, $\beta = 0.9$, $\varepsilon_{\mathrm{EPTT}}$ variation

The effect of $\varepsilon_{\mathrm{EPTT}}$ variation on radial stress ($\tau_{rr}$) are provided in Figure 9 by plotting ($\tau_{rr}$) along the top surface and the axis of symmetry with fixed {*We*=1, $\beta = 0.9$}. The profile of $\tau_{rr}$ reflects that its magnitude increases as $\varepsilon_{\mathrm{EPTT}}$ decreases. From $\varepsilon_{\mathrm{EPTT}} = 0.02$ to $\varepsilon_{\mathrm{EPTT}} = 0.25$, $\tau_{rr}$ reduces by about 70%, which implies that the effects of axial stress are important in this problem.

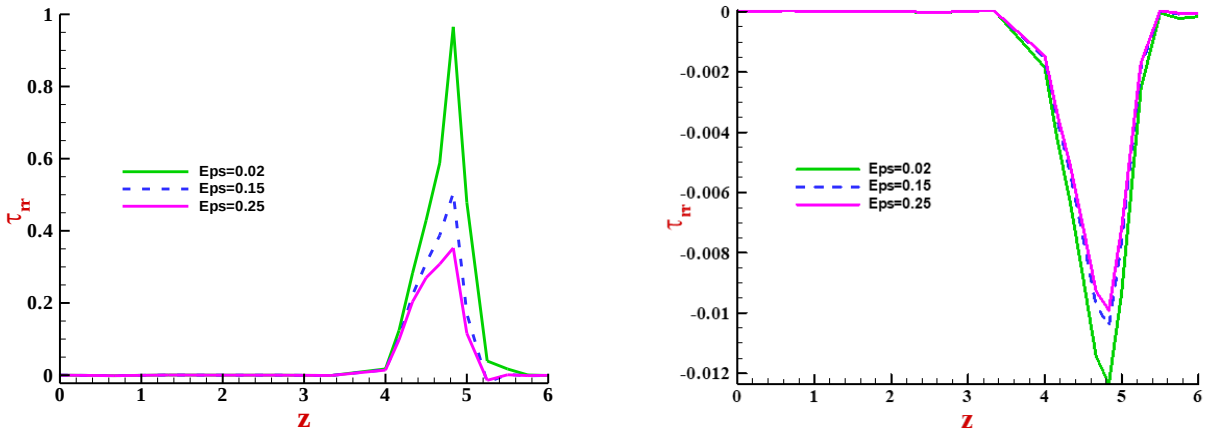


(a) Top Surface (b) Centreline

**Fig. 9.** Radial stress (τ_rr), EPTT{*We*=1, ξ_EPTT=0.0}: β=0.9, ε_EPTT variation

Studying the shear stress range ($\tau_{rz}$) can provide a complete feature about the history of deformation and the response of the fluid under consideration. Figure 10 displays the shear stress profiles under the same settings of parameters. Generally, a similar behaviour is observed in ($\tau_{rz}$)

with an opposite sign, where the magnitude of $\tau_{rz}$ decreases as $\varepsilon_{\mathrm{EPTT}}$ decreases because of the shear-thinning reflects

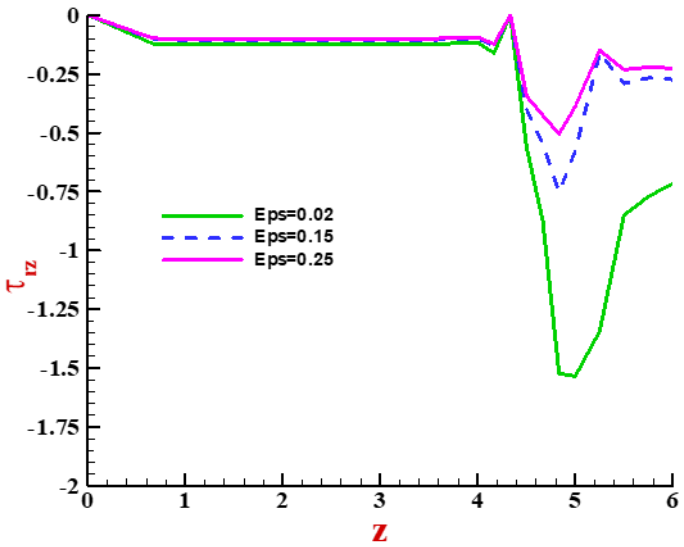


**Fig. 10.** Shear stress ($\tau_{rz}$) along the top wall, *EPTT*$\{We = 1, \xi_{\mathrm{EPTT}} = 0.0\}$: $\beta = 0.9$, $\varepsilon_{\mathrm{EPTT}}$-variation

For the same set of parameters, Figure 11 shows the normal stress ($\tau_{ZZ}$) along the top surface and the axis of symmetry. The results reveal that the normal constant stress levels occur along the die section and the outlet cone. They initially increase and then sharply decrease in the cone section. In both surfaces, the normal stress level increases as $\varepsilon_{\mathrm{EPTT}}$ decreases. The level of normal stress on the top surface is higher than that in the axis of symmetry.

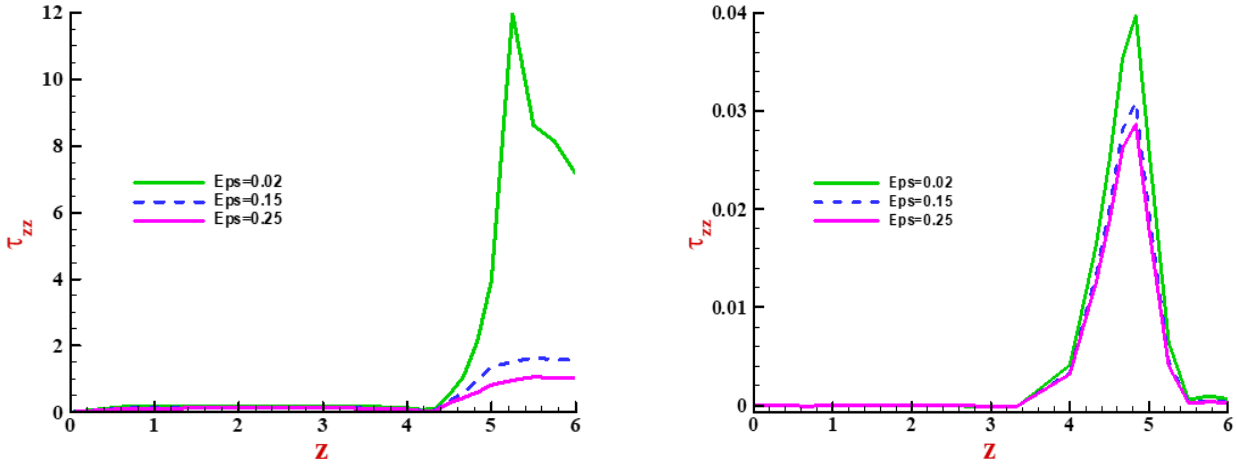


(a) Top Surface (b) Centreline

**Fig. 11.** Normal stress ($\tau_{zz}$), *EPTT*$\{We = 1, \xi_{\mathrm{EPTT}} = 0.0\}$: $\beta = 0.9$, $\varepsilon_{\mathrm{EPTT}}$ variation

## 6. Conclusion

This investigation covered the numerical solution of exponential Phan-Thien Tanner (EPTT) viscoelastic conical fluid. Conical channels are crucial to this study because it can help us understand how fluids behave in intricate geometries. This analysis advances our knowledge of fluid flow in conical channels and can help with the design and optimization of several industrial processes requiring similar by examining the effects of various parameters, such as $(We)$ and $\varepsilon_{\mathrm{EPTT}}$, on pressure drop and stress. Using a hybrid $FE/FV$ technique in a cylindrical coordinate system, we propose solutions for an axisymmetric conical issue with a shear-thinning viscoelastic EPTT model in this work. We research how $(We)$ and $\varepsilon_{\mathrm{EPTT}}$ have an impact. Our findings demonstrate that, when $(We)$ grows, the shear thinning qualities lead the degree of pressure drop to decrease and solvent fraction $\varepsilon_{\mathrm{EPTT}}$) to rise. We observe the same feature in radial stress, shear stress, and normal stress, which agree with other experimental results. We perform our study at three different levels of $\{\varepsilon_{\mathrm{EPTT}}\}$: $\varepsilon_{\mathrm{EPTT}} = 0.02$, $\varepsilon_{\mathrm{EPTT}} = 0.15$, and $\varepsilon_{\mathrm{EPTT}} = 0.25$. Here, we note a moderate effect on pressure drop and a significant effect of $\{\varepsilon_{\mathrm{EPTT}}\}$ on stress.

## References

[1] Harrison, W. J. "The pressure in a viscous liquid moving through a channel with diverging boundaries." In *Proc Cambridge Phil Soc*, vol. 19, pp. 307-312. 1919.
[2] Bond, W. N. "CXIV. Viscous flow through wide-angled cones." *The London, Edinburgh, and Dublin Philosophical Magazine and Journal of Science* 50, no. 299 (1925): 1058-1066. https://doi.org/10.1080/14786442508628550
[3] Oka, Syoten, and Akira Takami. "The steady slow motion of a non-Newtonian liquid through a tapered tube." *Japanese Journal of Applied Physics* 6, no. 4 (1967): 423.
[4] Forsyth, T. H. "Converging flow of polymers." *Polymer-Plastics Technology and Engineering* 6, no. 1 (1976): 101-131. https://doi.org/10.1080/03602557608055823
[5] Sutterby, John L. "Laminar converging flow of dilute polymer solutions in conical sections. II." *Transactions of the Society of Rheology* 9, no. 2 (1965): 227-241. https://doi.org/10.1122/1.549024
[6] Kwon, T. H., S. F. Shen, and K. K. Wang. "Pressure drop of polymeric melts in conical converging flow: Experiments and predictions." *Polymer Engineering & Science* 26, no. 3 (1986): 214-224. https://doi.org/10.1002/pen.760260306
[7] Kajiwara, T., S. Ninomiya, Y. Kuwano, and K. Funatsu. "Numerical simulation of converging flow of polymer melts through a tapered slit die." *Journal of non-newtonian fluid mechanics* 48, no. 1-2 (1993): 111-124. https://doi.org/10.1016/0377-0257(93)80067-L
[8] Jarzebski, A. B., and W. L. Wilkinson. "Non-isothermal developing flow of a generalised power-law fluid in a tapered tube." *Journal of Non-Newtonian Fluid Mechanics* 8, no. 3-4 (1981): 239-248. https://doi.org/10.1016/0377-0257(81)80023-7
[9] Settles, Gary S., and Hsueh-Ying Teng. "Cylindrical and conical flow regimes of three-dimensional shock/boundary-layer interactions." *AIAA journal* 22, no. 2 (1984): 194-200. https://doi.org/10.2514/3.8367
[10] Sutterby, J. L. "Laminar converging flow of dilute polymer solutions in conical sections: Part I. Viscosity data, new viscosity model, tube flow solution." *AIChE Journal* 12, no. 1 (1966): 63-68. https://doi.org/10.1002/aic.690120114
[11] Abdulhasan, Ahmed N., and Alaa H. Al-Muslimawi. "Numerical investigation of extensional flow through axisymmetric conical geometries: Finite element method." *Basrah Journal of Science* 38, no. 3 (2020): 399-421.
[12] Cogswell, F. N. "Converging flow and stretching flow: a compilation." *Journal of Non-Newtonian Fluid Mechanics* 4, no. 1-2 (1978): 23-38. https://doi.org/10.1016/0377-0257(78)85004-6
[13] Al-Muslimawi, A., H. R. Tamaddon-Jahromi, and M. F. Webster. "Simulation of viscoelastic and viscoelastoplastic die-swell flows." *Journal of Non-Newtonian Fluid Mechanics* 191 (2013): 45-56. https://doi.org/10.1016/j.jnnfm.2012.08.004
[14] Wapperom, P., and M. F. Webster. "A second-order hybrid finite-element/volume method for viscoelastic flows." *Journal of Non-Newtonian Fluid Mechanics* 79, no. 2-3 (1998): 405-431. https://doi.org/10.1016/S0377-0257(98)00124-4
[15] Aboubacar, M., H. Matallah, and M. F. Webster. "Highly elastic solutions for Oldroyd-B and Phan-Thien/Tanner fluids with a finite volume/element method: planar contraction flows." *Journal of Non-Newtonian Fluid Mechanics* 103, no. 1 (2002): 65-103. https://doi.org/10.1016/S0377-0257(01)00164-1

[16] Al-Muslimawi, A., H. R. Tamaddon-Jahromi, and M. F. Webster. "Numerical simulation of tube-tooling cable-coating with polymer melts." *Korea-Australia Rheology Journal* 25 (2013): 197-216. . https://doi.org/10.1007/s13367-013-0021-x

[17] Al-Muslimawi, Alaa H. "Numerical study for differential constitutive equations with polymer melts by using a hybrid finite-element/volume method." *Journal of Computational and Applied Mathematics* 308 (2016): 488-498. https://doi.org/10.1016/j.cam.2016.06.007

[18] Townsend, P., and M. F. Webster. "An algorithm for the three-dimensional transient simulation of non-Newtonian fluid flows." In *Proc. Int. Conf. Num. Meth. Eng.: Theory and Applications, NUMETA, Nijhoff, Dordrecht*, vol. 12, pp. 1-11. 1987.

[19] Matallah, H., P. Townsend, and M. F. Webster. "Recovery and stress-splitting schemes for viscoelastic flows." *Journal of Non-Newtonian Fluid Mechanics* 75, no. 2-3 (1998): 139-166. https://doi.org/10.1016/S0377-0257(97)00085-2

[20] Hasan, Zinah Abdulkadhim, and Abdul-Sattar J. Al-Saif. "A new approach to solving two-dimensional unsteady incompressible Navier-Stokes equations." *Journal of Applied Mathematics and Physics* 10, no. 10 (2022): 3218-3239.

[21] Aboubacar, M., H. Matallah, H. R. Tamaddon-Jahromi, and M. F. Webster. "Numerical prediction of extensional flows in contraction geometries: hybrid finite volume/element method." *Journal of non-newtonian fluid mechanics* 104, no. 2-3 (2002): 125-164. https://doi.org/10.1016/S0377-0257(02)00015-0

[22] Yasir, Reisan Y., Alaa H. Al-Muslimawi, and Bashaeer K. Jassim. "Numerical simulation of non-Newtonian inelastic flows in channel based on artificial compressibility method." *Journal of Applied and Computational Mechanics* 6, no. 2 (2020): 271-283.

[23] Al-Muslimawi, Alaa H. "Taylor Galerkin pressure correction (TGPC) finite element method for incompressible Newtonian cable-coating flows." *Journal of Kufa for Mathematics and Computer* 5, no. 2 (2018): 14-22. https://doi.org/10.31642/jokmc/2018/050203

[24] Al-Haboobi, Anas, and Alaa H. Al-Muslimawi. "Novel algorithm for compressible Newtonian axisymmetric thermal flow." *International Journal of Modern Physics C* 2450025 (2024): 17. https://doi.org/10.1142/S0129183124500256

[25] Sharhan, Alaa, and Alaa H. Al-Muslimawi. "Numerical Study of Shear and Extensional Inelastic Contraction Flows." *CFD Letters* 15, no. 8 (2023): 107-121. https://doi.org/10.37934/cfdl.15.8.107121

[26] Fadhel, Ihssan A., and Alaa H. Al-Muslimawi. "Numerical simulation of stick-slip viscoelastic fluid by using a hybrid finite-element/volume method." In *AIP Conference Proceedings*, vol. 2398, no. 1. AIP Publishing, 2022. https://doi.org/10.1063/5.0093620

[27] Fadhel, Ihssan Aqeel, and Alaa Hassan Al-Muslimawi. "Simulation of Oldroyd-B Viscoelastic Fluid in Axisymmetric Straight Channel by Using a Hybrid Finite Element/Volume Method." *Journal of Advanced Research in Fluid Mechanics and Thermal Sciences* 81, no. 1 (2021): 26-40.